ARTICLE

High Pressure Structural Instability and Thermal Properties of Rutile TiO_2 from First-principles

Cui-e Hu[a,b], Zhao-yi Zeng[a,b*], Chun-yang Kong[a], Yu-ting Cui[a], Lin Zhang[b], Ling-cang Cai[b]

a. College of Physics and Electronic Engineering, Chongqing Normal University, Chongqing 400047, China

b. National Key Laboratory for Shock Wave and Detonation Physics Research, Institute of Fluid Physics, Chinese Academy of Engineering Physics, Mianyang 621900, China

(Dated: Received on August 15, 2013; Accepted on November 11, 2013)

We report a first-principles calculation to investigate the structural instability of rutile TiO_2. The high pressure structural parameters are well reproduced. The calculated phonon dispersion curves agree with experiments at zero pressure. Under compression, we capture a large softening around Γ point, which indicates the structural instability. From the high pressure elastic constants, we find that the rutile TiO_2 is unstable when the applied pressure is larger than 17.7 GPa. Within the quasi-harmonic approximation, the thermal equation of state, thermal expansion coefficient, bulk modulus, and entropy are well reproduced. The thermal properties confirm the available experimental data and are extended to a wider pressure and temperature range.

Key words: TiO_2, Phonon dispersion, Thermodynamics, Density functional theory

I. INTRODUCTION

Titanium dioxide (TiO_2) has been widely used due to its versatile physical and chemical properties, such as in photoactive devices and biomaterials, high efficiency solar cells, super-hard materials, pigment, catalyst support, and photocatalyst [1−4]. TiO_2 crystallizes in several different forms: the rutile (space group $P42/mn$), anatase ($I4/amd$), brookite ($Pbca$), columbite ($Pbcn$), baddeleyite ($P21/c$), and cotunnite ($Pnma$) structures. The phase transitions of TiO_2 under pressure are of particular interest in Earth science, as these phases are an accessible analog of minerals in the Earth's mantle. Its physical properties have been vigorously pursued [5−15]. Montanari and Harrison [5] reported the influence of gradient corrections in density functional calculations, and they compared the local-density approximation (LDA) and two the generalized gradient approximation (GGA) results, including equilibrium structure, bulk modulus, and Γ-point phonons of bulk rutile TiO_2. Recently, Mei *et al.* investigated the lattice dynamics and thermodynamics of six TiO_2 polymorphs [16]. Mikami *et al.* studied the atomic and electronic structures of anatase and rutile phases of TiO_2 [17]. The pressure-induced phase transitions of TiO_2 were investigated by Wu *et al.* [7]. The calculated electronic properties show that all five polymorphs of TiO_2 they considered are semiconductors, and the lower conduction band is dominated by the 3d states of Ti that are sensitive to the coordination number of titanium.

Rutile TiO_2 is the most common natural form of TiO_2, and it is expected to undergo a sequence of phase transformations with increasing pressure. Rutile derives its name from the Latin rutilus, red, in reference to the deep red color observed in some specimens viewed by transmitted light. Rutile has the highest refractive indices of any known mineral and exhibits high dispersion. Its very high refractive index makes it an ideal white pigment and opacifier. Furthermore, rutile is a strong absorber of ultraviolet (UV) light, and is therefore used in solar cell technology. The rutile TiO_2 has been extensively studied from different aspects [5, 17−19].

The thermal equation of state (EOS) is a measurement of relationship between pressure, volume and temperature (P-V-T), which is a fundamental equation in many areas of basic and applied condensed-matter research. The pressure responses of the structural parameters and the phase transition induced by hydrostatic pressure in materials have been investigated extensively in the last decade [20], except the investigations on high pressure and high temperature. And we provide a systematic study of the thermal EOS of rutile TiO_2. In this work, we focus on the structure instability and thermodynamics of rutile TiO_2 under high pressure and high temperature through plane-wave pseudopotential density functional theory (DFT) method. The high pressure structures, elastic constants, phonon dispersions and thermodynamics of TiO_2 are presented and analyzed.

*Author to whom correspondence should be addressed. E-mail: zhaoyizeng@126.com

II. THEORETICAL METHOD

The high pressure structures, elastic constants and lattice dynamics calculations are implemented through the Cambridge Serial Total Energy Package (CASTEP) scheme [21]. The exchange and correlation potentials were treated within GGA of Perdew-Burke-Ernzerhof (PBE) [22]. The calculations were conducted with 18×18×18 Γ-centered k meshs. The plane-wave energy cutoff was 700 eV and the self-consistence convergence of the energy was set to 10^{-6} eV/atom. For the elastic constants, they are calculated as the second derivatives of the internal energy with respect to the strain tensor. These elastic constants can be determined by computing the stress generated by applying a small strain to an optimized unit cell. In practice, the maximum strain amplitude is set from −0.003 to 0.003 and all forces on atoms are converged to less than 0.006 eV/Å. For the phonon dispersion calculations, the dynamical matrices are computed at 66 wave (q) vectors in the irreducible wedge of Brillouin zone.

To obtain thermodynamic properties, we calculate the Helmholtz free energy F as follows

$$F(V,T) = E_{\rm static}(V) + F_{\rm phon}(V,T) + F_{\rm elec}(V,T) \quad (1)$$

where $E_{\rm static}(V)$ is the energy of a static lattice at zero temperature T and volume V, $F_{\rm elec}(V,T)$ is the thermal free energy arising from electronic excitations, and $F_{\rm phon}(V,T)$ is the phonon contribution. Both $E_{\rm static}(V)$ and $F_{\rm elec}(V,T)$ can be obtained from static first-principles calculations directly. The phonon vibrational contribution $F_{\rm phon}(V,T)$ has been calculated in the quasi-harmonic approximation (QHA)

$$F_{\rm phon}(V,T) = \frac{k_{\rm B}T}{\Omega}\int_{\rm BZ} {\rm d}q \sum_s \ln\left[2\sin\left(\frac{\hbar\eta\omega_{qs}}{2k_{\rm B}T}\right)\right] \quad (2)$$

where $\Omega=(2\pi)^3/V$ is the volume of the Brillouin zone, $k_{\rm B}$ is the Boltzmann constant, $\hbar$ is the Plank constant divided by 2π, and ω_{qs} is the phonon frequencies.

III. RESULTS AND DISCUSSION

A. Static structural properties

For rutile TiO_2, there are three independent structural parameters, *i.e.* the lattice paramerters a, c, and the cell-internal dimensionless parameter u, which denotes the position of the second atom along the c-axis. The calculated equilibrium lattice parameters are as follows: a=4.653 Å, c=2.975 Å, and u=0.305. Our results agree with the available experimental data [23, 24] and other theoretical results [7, 9, 16, 25, 26]. In comparison with the experimental data [23] (a=4.587 Å, c=2.954 Å, and u=0.305), the present lattice parameters are overestimated slightly (about 1%).

The static equation of state of rutile TiO_2 are obtained by fitting the energy-volume (E-V) data to the fourth-order finite strain EOS [27]. In Fig.1, we present the dependence of calculated normalized lattice parameters, including V/V_0, a/a_0, and c/c_0 (V_0, a_0, and c_0 are the zero pressure equilibrium lattice parameters) on pressure at zero temperature. It is seen that as pressure increases, the relative lattice parameters decrease linearly. Our results agree with the experimental data below 15 GPa [28−30]. From Fig.1, we can also find that the a-axis is much easier to compress than c-axis, which may be due to metal-metal repulsion parallel to c across the sharing doctahedral edge. As a consequence, the axial ratio c/a becomes larger under compression. For the internal parameter u, it shows a slight dependence on the pressure. By fitting the u-P data to a second-order polynomial, we have the following relations u=0.305−1.164×10^{-4}P+1.867×10$^{-6}P^2$. As the pressure increases to 25 GPa, u only decreases 0.57%.

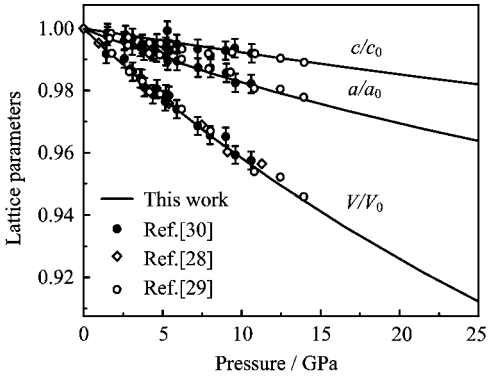

FIG. 1 Static lattice parameters of TiO_2 under high pressure, together with the experimental data.

We calculate the phonon dispersions of rutile TiO_2 at different pressures. As there are 6 atoms in a primitive cell, there should be 15 optical modes and 3 acoustic modes. Figure 2 shows the obtained high pressure phonon dispersion curves of rutile TiO_2 along several high symmetry directions in the Brillouin zone. From Fig.2, one can see that the phonon frequencies at zero pressure agree with the inelastic neutron scattering data [31]. As pressure increases, most of the phonon frequencies increase, except the values around Γ point. As pressure increases, the softening of dispersions becomes more and more obvious. Under ultra compression (∼20 GPa), the frequencies around Γ point soften to imaginary frequencies, indicating a structural instability. Actually, under this pressure, the rutile phase is mechanically instable.

B. Elastic properties

Elastic moduli are the material constants that connect stress with strain and are therefore crucial to engineer applications. They also determine the long wavelength vibrational modes, or sound waves, in a solid. We calculate the elastic constants of TiO_2 under high

DOI:10.1063/1674-0068/27/01/69-74

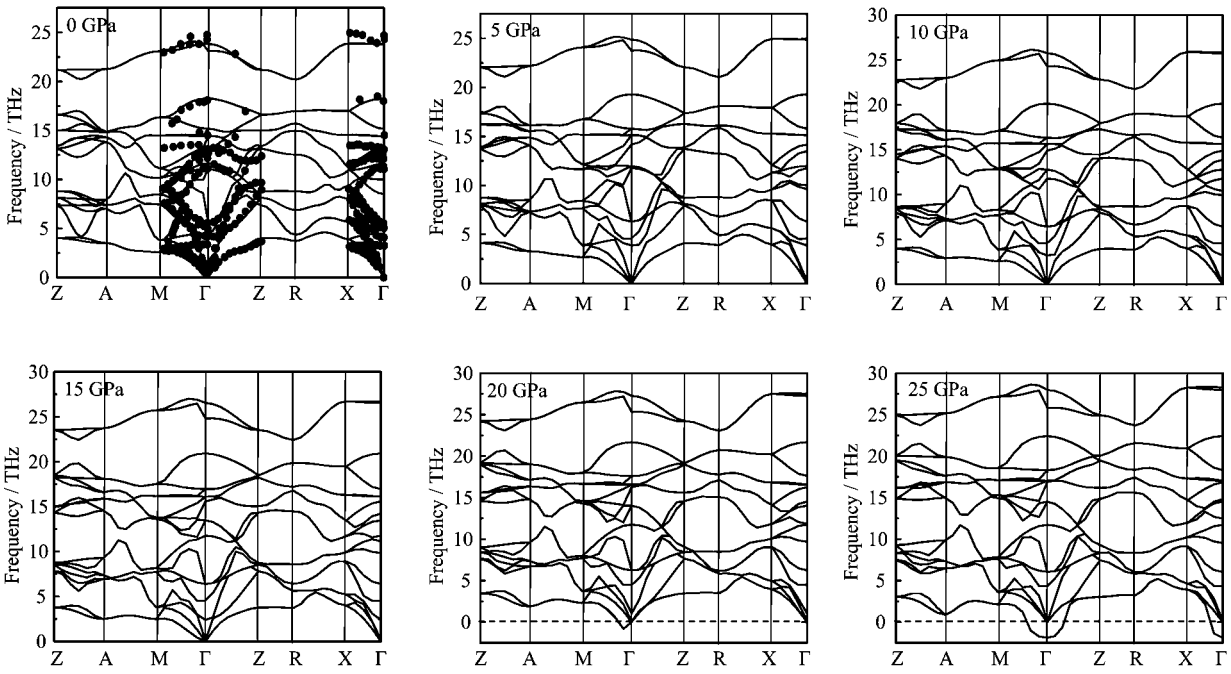

FIG. 2 The phonon dispersion curves of rutile TiO_2 under different pressure of 0, 5, 10, 15, 20, and 25 GPa, together with the experimental data at zero pressure (solid spheres) [31].

TABLE I Calculated high pressure elastic constants C_{ij} (in GPa). The C_S=C_{11}−C_{12}−2P (in GPa) is the mechanical instability criterion.

P/GPa	C_{11}	C_{33}	C_{44}	C_{66}	C_{12}	C_{13}	C_S
0	289.51	463.13	111.4	229.45	183.95	165.6	105.56
5	319.71	491.59	114.63	249.63	217.13	192.7	92.58
10	339.78	517.39	114.42	267.19	246.8	215.44	72.98
15	356.96	540.15	114.81	286.69	293.18	234.89	33.78
20	392.49	564.27	112.58	301.66	299.43	257.98	53.06
25	418.14	592.91	117.29	316.96	327.25	280.36	40.89

TABLE II Aggregate elastic moduli B, G, Y, the Poisson's ratio σ, and sound velocities V_P, V_S, and V_B of rutile TiO_2.

P/GPa	B/GPa	G/GPa	Y/GPa	σ	V_S/(km/s)	V_P/(km/s)	V_B/(km/s)
0	223.01	69.05	187.76	0.364	4.083	8.722	7.338
5	253.11	69.01	190.04	0.379	4.042	9.035	7.736
10	277.33	66.28	184.17	0.395	3.921	9.211	8.021
15	304.5	57.56	162.45	0.409	3.623	9.324	8.333
20	326.33	66.36	186.43	0.407	3.859	9.649	8.559
25	351.64	67.08	189.22	0.582	3.852	9.877	8.819

pressure (Table I). The theoretical polycrystalline elastic modulus can be determined from the independent elastic constants.

The average isotropic shear modulus G and bulk modulus B of polycrystalline (Table II) can be calculated according to Voigt-Reuss-Hill approximations [32]. Then the isotropically averaged aggregate velocities can be obtained as follows

$$V_P = \left(\frac{B + 4G/3}{\rho}\right)^{1/2} \tag{3}$$

$$V_S = (G/\rho)^{1/2} \tag{4}$$

$$V_B = (B/\rho)^{1/2} \tag{5}$$

where ρ is the density, V_P, V_S, and V_B are the compressional, shear, and bulk sound velocities, respectively (Table II). The V_P and V_B increase monotonously with the increasing pressure. But for the V_S, the abnormal variation locates between 15 and 20 GPa, which results in the variation of shear modulus.

The polycrystalline Young's modulus Y and the Pois-

DOI:10.1063/1674-0068/27/01/69-74

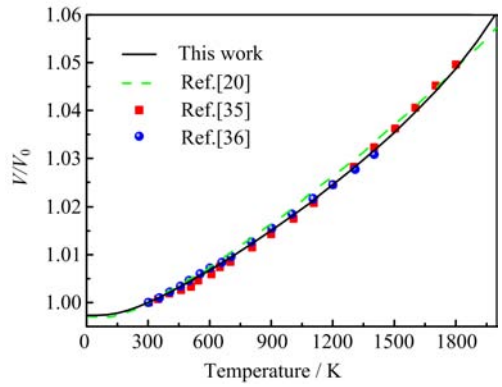

FIG. 3 The normalized volume V/V_0 (V_0 is the volume at 300 K) versus temperature at 0 GPa, together with the previous theoretical results [20] and experimental data [35, 36].

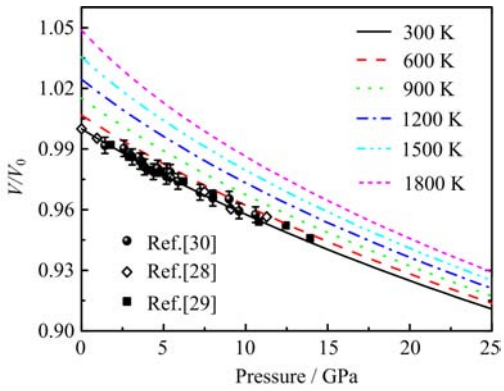

FIG. 4 The normalized volume V/V_0 versus pressure at different temperatures, together with the experimental data [28−30].

son's ratio σ are then calculated from B and G as follows

$$Y = \frac{9BG}{3B+G} \tag{6}$$

$$\sigma = \frac{3B-2G}{2\,(3B+G)} \tag{7}$$

From Tables I and II, we can find all the elastic constants C_{ij} and bulk modules B increase as pressure rises. But the shear modulus G and Young's modulus Y decrease with the increasing pressure up to 15 GPa. When the pressure is larger than 20 GPa, the two moduli increase with the increasing pressure. The calculated σ is also shown in Table II. At zero pressure, σ is 3.36. As the pressure rise, σ increases to 0.41 at 15 GPa. The value at 20 GPa nearly equals to that at 15 GPa. But when the pressure increases to 25 GPa, σ is larger than the liquid value of 0.5, which is physically implausible since TiO_2 is a solid.

Under isotropic pressure, the mechanical stability is judged by the following condition [33]

$$\tilde{C}_{44} > 0, \quad \tilde{C}_{11} > |\tilde{C}_{12}|, \quad \tilde{C}_{11} + 2|\tilde{C}_{12}| > 0 \tag{8}$$

$$\tilde{C}_{\alpha\alpha} = C_{\alpha\alpha} - P \quad (\alpha = 1, 3, 4) \tag{9}$$

$$\tilde{C}_{12} = C_{12} + P \tag{10}$$

$$\tilde{C}_{13} = C_{13} + P \tag{11}$$

Though these criterions are suited for rutile TiO_2 in the whole applied pressure range, the C_S ($C_{11}-C_{12}-2P$), can be divided into two opposite variations with the pressure rising. At the pressure range from 0 GPa to 15 GPa, the C_S decreases monotonously with the increasing pressure. If we extrapolate the C_S to high pressure, when P=17.7 GPa, C_S=0, indicating that the rutile TiO_2 is unstable when the applied pressure is larger than 17.7 GPa. From the high pressure elastic constants, we can judge that the phase transition of TiO_2 from rutile structure to the other structure should occur around 17.7 GPa. Actually, at room temperature, according to the X-ray experiments, rutile is stable up to 12 GPa, where a direct transition to baddeleyite-type phase takes place [34].

C. Thermodynamics

Then we focus on the thermodynamic properties of rutile TiO_2 under high pressure and temperature. The accurate thermodynamic properties as functions of pressure and temperature can directly provide the valuable information for understanding the phase diagram and dynamical response of materials under extreme conditions. The inclusion of temperature makes P-V-T EOS more important than P-V EOS. The normalized volume V/V_0 (V_0 is the volume at 300 K) at zero pressure is shown in Fig.3. The volume increases with the increasing temperature. Considering the temperature contribution to the free energy at 300 K, it increases the equilibrium volume by 0.27% with respect to the static value. When the temperature reaches up to 2000 K (near the melting point), the volume expands 6% compared with the static value. The present results agree well with the previous theoretical results [20] and experimental data [35, 36] (see Fig.3). The volumes of rutile TiO_2 under high pressure and high temperature are shown in Fig.4. One notes the 300 K isotherm is almost the same as the one at 0 K (shown in Fig.1) and this is due to the small free energy contribution from the lattice vibrations at 300 K. Our isotherms agree well with the experimental data [28−30] with increasing pressure. When the temperature goes from 300 K to 1800 K, the contribution of vibrational free energy becomes larger and larger.

The volume thermal expansion coefficient is determined from the equilibrium volume variation with respect to the temperature at each pressure.

$$\alpha_V = \frac{1}{V}\left(\frac{\partial V}{\partial T}\right)_P \tag{12}$$

In Fig.5, we plot the thermal expansion coefficient as

DOI:10.1063/1674-0068/27/01/69-74

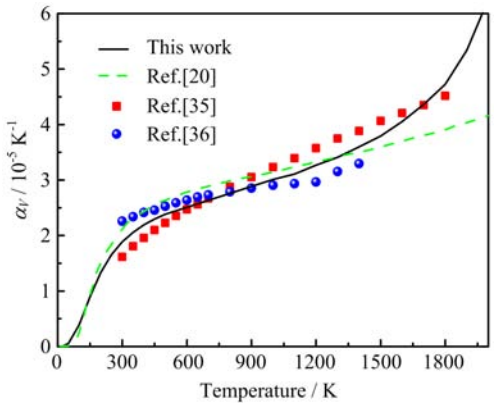

FIG. 5 Thermal expansion coefficient α_V versus temperature at 0 GPa, together with the previous theoretical results [20], and experimental data [35, 36].

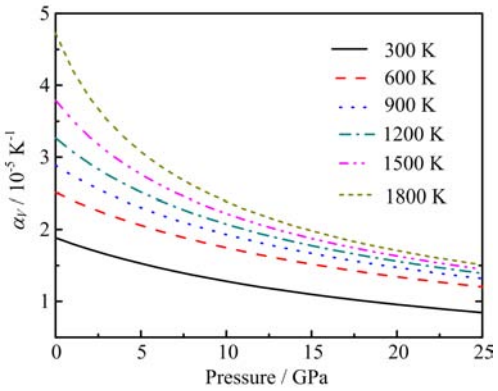

FIG. 6 Thermal expansion coefficient α_V versus pressure at different temperatures.

a function of temperature at 0 GPa. At zero pressure, the predicted temperature dependence of the thermal expansion coefficient appears to be significantly based on the QHA. Our results agree with the previous theoretical results [20] and experimental data [35, 36]. At 300 K, the calculated α_V is 1.88×10^{-5} K^{-1}. At high temperature (above 1400 K), our results seem much better than that from Francisco *et al.* [20]. The thermal expansion coefficients as functions of pressure at different temperatures are shown in Fig.6. As pressure rises, the thermal expansion is suppressed quickly. That is to say the pressure can suppress part of anharmonicity by strengthening the bondings among atoms and lowering the vibration of atoms. Thus under pressure, the validity of quasi-harmonic approximation can be extended to much higher temperature.

The investigation on the entropy S of crystals is an old topic of condensed matter physics, which can provide essential insight into the vibrational properties. As shown in Fig.7, the calculated S of rutile TiO_2 are in general agreement with the theoretical results [16] and the experimental data [37]. The entropies are somewhat underestimated. However, the largest difference

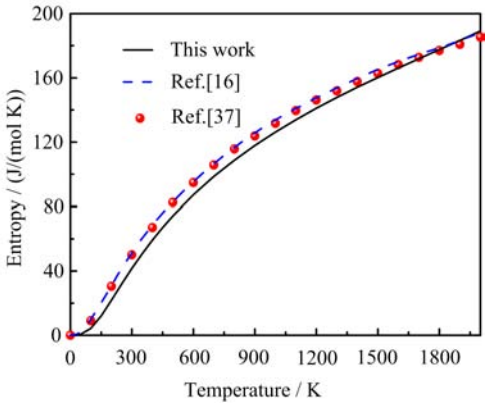

FIG. 7 Entropy S versus temperature at 0 GPa, together with the theoretical results [16] and experimental data [37].

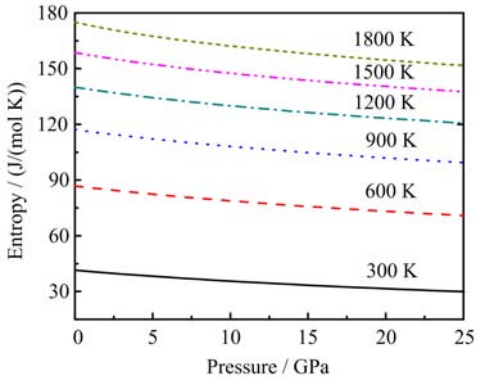

FIG. 8 Entropy S versus pressure at different temperatures.

between our results and the experimental data is less than 7%. Figure 8 shows the predicted entropy S under pressure. The entropies decrease slightly with the increasing pressure.

IV. CONCLUSION

In summary, we employ first-principles calculations to investigate the structural instability and thermodynamics of rutile TiO_2. The high pressure structural parameters of TiO_2 are well reproduced. The calculated phonon dispersion curves agree with experiments at zero pressure. Under compression, we capture a large softening around Γ point. When the pressure is raised to 20 GPa, the frequencies around Γ point in transverse acoustical branches become imaginary, indicating the structural instability. From the high pressure elastic constants obtained, we find that the rutile TiO_2 is unstable when the applied pressure is larger than 17.7 GPa. Within the quasi-harmonic approximation, the thermal equation of state, thermal expansion coefficient, bulk modulus and entropy are well reproduced. The thermal properties confirm the available experimental data and are extended to a wider pres-

DOI:10.1063/1674-0068/27/01/69-74

sure and temperature range.

V. ACKNOWLEDGMENTS

This work was supported by the National Natural Science Foundation of China (No.11247316, No.11247317, and No.11304408), the Science and Technology Research Project of Chongqing Education Committee (No.KJ120613 and No.KJ130607), and the Natural Science Foundation of Chongqing City (No.cstc2012jjA50019 and No.cstc2013jcyjA0733).

[1] V. Swamy, B. C. Muddle, and Q. Dai, Appl. Phys. Lett. **89**, 163118 (2006).
[2] R. Asahi, T. Morikawa, T. Ohwaki, K. Aoki, and Y. Taga, Science **293**, 269 (2001).
[3] Y. Gai, J. Li, S. S. Li, J. B. Xia, and S. H. Wei, Phys. Rev. Lett. **102**, 036402 (2009).
[4] H. G. Yang, C. H. Sun, S. Z. Qiao, J. Zou, G. Liu, S. C. Smith, H. M. Cheng, and G. Q. Lu, Nature **453**, 638 (2008).
[5] B. Montanari and N. M. Harrison, Chem. Phys. Lett. **364**, 528 (2002).
[6] J. S. Olsen, L. Gerward, and J. Z. Jiang, J. Phys. Chem. Solids **60**, 229 (1999).
[7] X. Wu, E. Holbig, and G. Steinle-Neumann, J. Phys.: Condens. Matter **22**, 295501 (2010).
[8] Y. Al-Khatatbeh, K. K. M. Lee, and B. Kiefer, Phys. Rev. B **79**, 134114 (2009).
[9] B. Montanari and N. M. Harrison, J. Phys.: Condens. Matter **16**, 273 (2004).
[10] M. Giarola, A. Sanson, F. Monti, and G. Mariotto, Phys. Rev. B **81**, 174305 (2010).
[11] E. Shojaee, M. Abbasnejad, M. Saeedian, and M. R. Mohammadizadeh, Phys. Rev. B **83**, 174302 (2011).
[12] M. Mattesini, J. S. D. Almeida, L. Dubrovinsky, N. Dubrovinskaia, B. Johansson, and R. Ahuja, Phys. Rev. B **70**, 115101 (2004).
[13] H. Sato, S. Endo, M. Sugiyama, T. Kikegawa, and O. Shimomura, Science **251**, 786 (1991).
[14] T. Mashimo, K. Nagayama, and A. Sawaoka, J. Appl. Phys. **54**, 5043 (1983).
[15] R. Miloua, Z. Kebbab, N. Benramdane, M. Khadraoui, and F. Chiker, Comp. Mater. Sci. **50**, 2142 (2011).
[16] Z. G. Mei, Y. Wang, S. L. Shang, and Z. K. Liu, Inorg. Chem. **50**, 6996 (2011).
[17] M. Mikami, S. Nakamura, O. Kitao, H. Arakawa, and X. Gonze, Jpn. J. Appl. Phys. **39**, L847 (2000).
[18] R. Sikora, J. Phys. Chem. Solids **66**, 1069 (2005).
[19] P. D. Mitev, K. Hermansson, B. Montanari, and K. Refson, Phys. Rev. B **81**, 134303 (2010).
[20] E. Francisco, M. Bermejo, V. G. Baonza, L. Gerward, and J. M. Recio, Phys. Rev. B **67**, 064110 (2003).
[21] M. D. Segall, P. J. D. Lindan, M. J. Probert, C. J. Pickard, P. J. Hasnip, S. J. Clark, and M. C. Payne, J. Phys.: Condens. Matter **14**, 2717 (2002).
[22] J. P. Perdew, K. Burke, and M. Ernzerhof, Phys. Rev. Lett. **77**, 3865 (1996).
[23] J. K. Burdett, T. Hughbanks, G. J. Miller, J. W. Richardson, and J. V. Smith, J. Am. Chem. Soc. **109**, 3639 (1987).
[24] Y. Kudoh and H. Takeda, Physica B+C **139**, 333 (1986).
[25] J. X. Yu, M. Fu, G. F. Ji, and X. R. Chen, Chin. Phys. B **18**, 0269 (2009).
[26] R. Shirley, M. Kraft, and O. R. Inderwildi, Phys. Rev. B **81**, 075111 (2010).
[27] F. Birch, J. Geophys. Res. **91**, 4949 (1986).
[28] Y. Al-Khatatbeh, K. K. M. Lee, and B. Kiefer, Phys. Rev. B **79**, 134114 (2009).
[29] L. Gerward and J. S. Olsen, J. Appl. Crystallogr. **30**, 259 (1997).
[30] L. Ming, and M. H. Manghnani, J. Geophys. Res. **84**, 4777 (1979).
[31] J. G. Traylor, H. G. Smith, R. M. Nicklow, and M. K. Wilkinson, Phys. Rev. B **3**, 3457 (1971).
[32] R. Hill, Proc. Phys. Soc. London **65**, 350 (1952).
[33] G. V. Sińko and N. A. Smirnov, J. Phys.: Condens. Matter **14**, 6989 (2002).
[34] J. S. Olsen, L. Gerward, and J. Z. Jiang, J. Phys. Chem. Solids **60**, 229 (1999).
[35] S. K. Saxena, N. Chatterjee, Y. Fei, and G. Shen, *Thermodynamic Data on Oxides and Silicates: An Assessed Data Set Based on Thermochemistry and High-Pressure Phase Equilibrium*, Berlin: Springer-Verlag, (1993).
[36] Y. S. Touloukian, R. K. Kirby, R. E. Taylor, and T. Y. R. Lee, *Thermophysical Properties of Matter*, New York: IFI/Plenum, 13, (1977).
[37] M. W. Chase, *NIST-JANAF Thermochemical Tables*, Washington, DC: American Institute of Physics, 2 (1998).

DOI:10.1063/1674-0068/27/01/69-74